Influence of substituents in bis(2-amino-5-*R*-phenyl)disulfide on the deposition processes and properties of nickel-phosphorus coatings

V.A. Polikarchuk, M.S. Derkachev, N.V. Sotskaya, N.S. Buylov and Kh.S. Shikhaliev*

Voronezh State University, 1 Universitetskaya pl., 394018 Voronezh, Russian Federation
**E-mail: shikh1961@yandex.ru*

Abstract

The research explored the effect of bis(2-aminophenyl)disulfide and their derivatives on the electroless nickel plating process and the characteristics of Ni–P coatings with corrosion-resistant properties. A method for synthesizing bis(2-amino-5-*R*-phenyl)disulfides with *R* substituents (H, CH_3, CH_3O, F, Cl, COOH, SO_3Na) at the 5th position from readily available materials was outlined. It was shown that all additives exhibit inhibitory effects on the bulk solution reaction, intensifying with higher concentrations. The additives exhibit both catalytic and inhibitory properties during the deposition of Ni–P coatings. An optimal range of additive concentrations ($1\cdot10^{-5}$–$3.16\cdot10^{-5}$ mol/L) was chosen to enhance coating deposition rates and solution stability. The effect of the substituent in additives becomes more evident during the coating formation, triggering modifications in composition, structure, and morphology. As additive concentrations rise, most substituents in them lead to decreased phosphorus content in the coating, except for *R* (CH_3 and SO_3Na). Comparatively weak reflections from the Ni(200) plane are noticeable in the X-ray diffraction patterns of coated surfaces, hinting at enhanced crystallinity in the deposit. The noteworthy effect of substituents at the 5th position of bis(2-amino-5-*R*-phenyl) disulfides is reflected in alterations in the morphology of the coatings. Depending on the concentration and substituents in the benzene ring, coatings appear either smoother for *R* (CH_3O, COOH, and SO_3Na) relative to additives absence, or exhibit a more developed surface for *R* (H, F, Cl).

Received: June 11, 2024. Published: July 11, 2024 doi: 10.17675/2305-6894-2024-13-3-5

Keywords: *Ni–P coating, electroless nickel deposition, stabilizers, accelerators, disulfides, bis(2-amino-5-R-phenyl)disulfides.*

1. Introduction

The process of electroless nickel plating has gained wide popularity since their development by Brenner and Riddell [1] in the mid-20th century. The utilization of phosphorus derivatives or their salts as reducing agents results in the formation of Ni–P alloys, enhancing the functional properties of coatings including corrosion resistance, hardness, and wear

resistance, among other characteristics. This is widely used in microelectronics, mechanical engineering, chemical, aerospace and textile industries [2–5].

Significant advantages of this process over electroplating include the ability to partially or fully cover surfaces of complex shapes with uniform thickness, direct deposition on surface-activated non-conductors, and the formation of less porous and more corrosion-resistant deposits. However, the process is autocatalytic, making electroless nickel plating baths highly sensitive to impurities that can affect the properties of the catalytic surface and promote unwanted side reactions in the solution, leading to solution self-decomposition. Therefore, to prevent sudden electrolyte decomposition, stabilizers need to be added. By the mechanism of action, stabilizers are usually divided into two categories. The first acts through a displacement mechanism, where metal ions (Pb^{2+}, Sn^{2+}, Cd^{2+}, Cu^{2+} and Fe^{2+}) are deposited on the active substrate surface as a result of a displacement reaction and can prevent random reduction of Ni^{2+}. However, the use of such stabilizers may lead to the co-deposition of certain elements, negatively affecting the coating properties. The other category operates through an adsorption mechanism [6], where hydrogen sulfide, sulfide, arsenide, and iodide ions can inhibit nickel deposition by adsorbing onto catalytic sites on the metal surface. This category includes sulfur organic compounds such as thiourea, cysteine, methionine, thioglycolic acid, 2-mercaptobenzimidazole, 2-mercaptobenzo-thiazole, which are increasingly used as stabilizers in electroless deposition processes [7–11]. Furthermore, it has been found that in addition to their stabilizing effect, these compounds exhibit an accelerating effect. It is believed that their accelerating action occurs by weakening the bond between hydrogen and phosphorus atoms in the hypophosphite molecule.

In previous studies [12, 13], a comparison was made on the influence of certain sulfur, nitrogen, and oxygen-containing organic compounds on the oxidation of hypophosphite. As a result, it was found that the catalytic effect is characteristic only for sulfur-containing compounds at low concentrations, accompanied by a shift in the stationary potential towards the negative side, which may be associated with surface modification and changes in the metal-hydrogen bond energy. It was also discovered that within a certain concentration range, organic compounds such as the disodium salt of 4,4′-dithiobenzenedisulfonic acid and 2,2′-diaminodithiobenzene with –S–S– fragments inhibit the homogeneous reaction and exhibit an accelerating effect on the surface reaction [14].

The aim of this study is to synthesize new bis(2-amino-5-*R*-phenyl)disulfides containing substituents of different electronic nature at the 5^{th} position of the benzene ring and to investigate their influence as additives on the deposition rate and physicochemical properties of Ni–P coatings, as well as the stability of the electroless nickel plating electrolyte.

2. Experimental

2.1. Synthesis of bis(2-amino-5-R-phenyl)disulfides

In the initial stage of this study, the synthesis of substituted 2-aminobenzo[*d*]thiazoles **2a–g** was conducted by reacting commercially available anilines **1a–g** with ammonium rhodanide and bromine in acetic acid [15–18]. As a result, the corresponding 6-*R*-2-aminobenzothiazoles **2a–f** were obtained in good yields of 72–85% (Figure 1).

Unfortunately, obtaining 2-aminobenzo[*d*]thiazole-6-sulfonic acid **2g** in this way led to the acylation product of the starting aniline at the amino group. However, direct selective sulfonation of unsubstituted 2-aminobenzo[*d*]thiazole **2a** by heating in concentrated sulfuric acid according to references [19, 20] results in the formation of sulfonic acid **2g** (Figure 1). Yields and melting temperatures of 6-*R*-2-aminobenzo[*d*]thiazoles **2a–g** are given in Table 1.

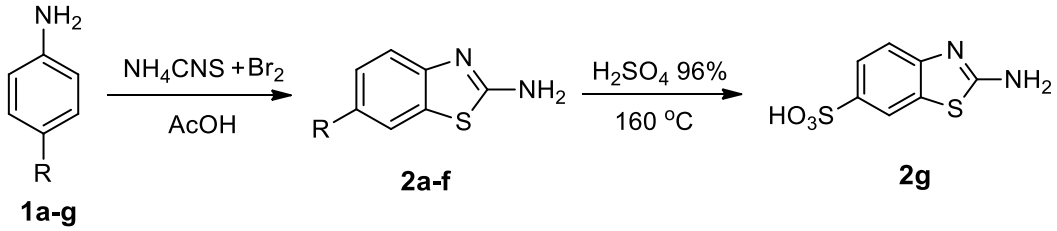

a R=H, **b** R=CH_3O, **c** R=Cl, **d** R=F, **e** R=COOH, **f** R=CH_3, **g** R=SO_3H

Figure 1. The synthesis scheme of 6-R-2-aminobenzo[d]thiazoles **2a–g**.

Table 1. Yields of 6-*R*-2-aminobenzo[*d*]thiazoles **2a–g**.

Compound	*R*	Yield, %	m.p., °C	m.p., °C (lit)
2a	H	75	133–134	130–131
2b	CH_3O	73	169–170	166–168
2c	Cl	81	200–202	197–199
2d	F	72	180–181	183–185
2e	COOH	85	265 (decomp.)	265 (decomp.)
2f	CH_3	72	122–124	126–128
2g	SO_3H	80	>300	No data

Subsequent refluxing of compounds **2a–g** in an aqueous solution of KOH or NaOH led to the formation of the corresponding 2-aminophenothiols **3a–g**, which were further subjected to mild oxidation by refluxing and stirring in an aqueous solution of sodium thiosulfate [21, 22]. As a result, bis(5-*R*-2-aminophenyl)disulfides **4a–g** were isolated with yields of 66–85% (Figure 2), which were subsequently investigated as additives in the electroless nickel deposition process.

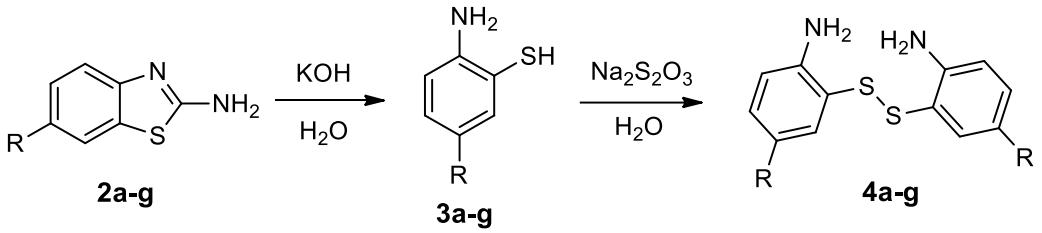

a R=H, **b** R=CH_3O, **c** R=Cl, **d** R=F, **e** R=COOH, **f** R=CH_3, **g** R=SO_3Na

Figure 2. The synthesis scheme of bis(2-amino-5-*R*-phenyl)disulfides **4a–g**.

Table 2. Yields of bis(2-amino-5-*R*-phenyl)disulfides **4a–g**.

Compound	*R*	Yield, %
4a	H	84
4b	CH_3O	75
4c	Cl	81
4d	F	72
4e	COOH	85
4f	CH_3	81
4g	SO_3Na	66

*General procedure for the synthesis of 6-R-2-aminobenzo[d]thiazoles **2a–f***

Bromine (0.56 ml, 11 mmol) was added dropwise to a suspension of NH_4SCN (1.7 g, 22 mmol) in AcOH (50 ml) at 10°C, and the reaction mixture was stirred at this temperature for 0.5 hours. After filtering out the insoluble materials, the filtrate was added to a solution of 4-*R*-aniline **1a–f** (10 mmol) in AcOH (50 ml) and the reaction mixture was stirred at 10°C for 19 hours. The solvent was evaporated under vacuum, and the resulting residue was diluted with water (100 ml). The pH of the mixture was adjusted to 1.0 with an HCl solution. After filtering out insoluble materials, the filtrate was made alkaline with NaOH until the precipitation ceased. The solid product was collected by filtration and crystallized from a hexane/AcOEt mixture.

*Synthesis of 2-aminobenzo[d]thiazole-6-sulfonic acid **2g***

3.0 g (0.02 mol) 2-aminobenzothiazole **2a** was dissolved in 10.0 ml 96% sulfuric acid (0.18 mol). The mixture was heated at 160°C for 35 min, cooled to room temperature and poured into cold water. The precipitate that formed was washed three times with water (10 ml) by decantation and filtered. The product was washed again with water.

*General procedure for the synthesis of bis(2-amino-5-R-phenyl)disulfides **4a–f***

A mixture of 10 mmol 2-aminobenzothiazole **2a–f** and (2.2 ml, 40 mmol) ethylene glycol were stirred in a 60 ml aqueous solution of KOH (6.0 M) at 140°C for 24 hours. After cooling, the solution was neutralized with concentrated HCl in an ice bath, the precipitate was filtered and washed with water. The resulting 2-amino-4-*R*-thiophenol **3a–f** and 2.5 g (0.01 mol) sodium thiosulfate pentahydrate are dispersed in 15 ml of water and the mixture was refluxed with stirring for 2 hours. After cooling to 20°C, the precipitate was filtered and crystallized from H_2O/EtOH mixture.

*Bis(2-aminophenyl)disulfide **4a***

Yield 2.1 g (84%), yellow solid, m.p. 87–89°C. ^{1}H NMR spectrum, 600 MHz, DMSO-d_6, δ, ppm (J, Hz): 3.73 (4H, br. s, NH_2), 6.43 (2H, t, *J*=7.5, 5-H), 6.72 (2H, d, *J*=8.1, 3-H), 6.98 (2H, d, *J*=7.7, 6-H), 7.08 (2H, t, *J*=7.7, 4-H). Found, *m/z*: 249.0510 $[M+H]^+$. $C_{12}H_{12}N_2S_2$. Calculated, *m/z*: 249.0515.

*Bis(2-amino-5-methoxyphenyl)disulfide **4b***

Yield 2.3 g (75%), green solid, m.p. 73–75°C. ^{1}H NMR spectrum, 600 MHz, DMSO-d_6, δ, ppm (J, Hz): 3.53 (6H, s, OCH_3), 5.03 (4H, s, NH_2), 6.60 (2H, d, *J*=2.8, 6-H), 6.70 (2H, d, *J*=8.8, 3-H), 6.77 (2H, d.d, *J*=8.8, 2.9, 4-H). Found, *m/z*: 309.0730 $[M+H]^+$. $C_{14}H_{16}N_2O_2S_2$. Calculated, *m/z*: 309.0727.

*Bis(2-amino-5-chlorophenyl)disulfide **4c***

Yield 2.6 g (81%), light green solid, m.p. 111–113°C. ^{1}H NMR spectrum, 600 MHz, DMSO-d_6, δ, ppm (J, Hz): 5.70 (4H, s, NH_2), 6.75 (2H, d, *J*=8.7, 3-H), 6.90 (2H, d, *J*=2.5, 6-H), 7.13 (2H, d.d, *J*=8.7, 3.5, 4-H). Found, *m/z*: 316.9734 $[M+H]^+$. $C_{12}H_{10}Cl_2N_2S_2$. Calculated, *m/z*: 316.9737.

*Bis(2-amino-5-fluorophenyl)disulfide **4d***

Yield 2.0 g (72%), dark green solid, m.p. 75–77°C. ^{1}H NMR spectrum, 600 MHz, DMSO-d_6, δ, ppm (J, Hz): 5.35 (4H, br. s, NH_2), 6.73 (2H, d.d, *J*=8.6, 5.2, 3-H), 6.83 (2H, d.d, *J*=8.6, 2.9, 6-H), 6.98 (2H, t.d, *J*=8.6, 2.9, 2H, 4-H). Found, *m/z*: 285.0325 $[M+H]^+$. $C_{12}H_{10}F_2N_2S_2$. Calculated, *m/z*: 285.0327.

*Bis(3,3′-disulfide-4-aminobenzoic acid) **4e***

Yield 2.9 g (85%), light yellow solid, m.p. 286°C (decomp.). ^{1}H NMR spectrum, 600 MHz, DMSO-d_6, δ, ppm (J, Hz): 7.35 (2H, d, *J*=8.4, 5-H), 7.80 (1H, d.d, *J*=8.4, 1.8, 6-H), 7.87 (4H, br. s, NH_2), 8.25 (2H, d, *J*=1.7, 2-H), 12.55 (1H, br. s, OH). Found, *m/z*: 337.0314 $[M+H]^+$. $C_{14}H_{12}N_2O_4S_2$. Calculated, *m/z*: 337.0312.

*Bis(2-amino-5-methylphenyl)disulfide **4f***

Yield 2.2 g (81%), light yellow solid, m.p. 78–80°C. ^{1}H NMR spectrum (400 MHz, DMSO-d_6), δ, ppm (J, Hz): 2.08 (6H, s, CH_3), 4.98 (4H, s, NH_2), 6.81 (2H, s, 3-H), 6.62 (2H, d, J=8.2, 6-H), 6.87 (2H, d.d, J=8.2, 1.6, 4-H). Found, m/z: 277.0823 $[M+H]^+$. $C_{14}H_{16}N_2S_2$. Calculated, m/z: 277.0828.

*Synthesis of disodium bis(3,3'-disulfide-4-aminobenzenesulfonate) **4g***

A mixture of 1.5 g (10 mmol) 2-aminobenzothiazole 2 g and (2.2 ml, 40 mmol) ethylene glycol in a NaOH aqueous solution (2.0 M, 60 ml) were stirred at 140°C for 2 hours. After cooling to 20°C, the solution was neutralized with concentrated HCl in an ice bath. Then, 2.5 g (0.01 mol) of sodium thiosulfate pentahydrate were added to the solution, and the mixture was refluxed with stirring for 2 hours. The solvent was evaporated at 60°C under vacuum until the precipitation began, which was then filtered. The the crude product was dried and extracted with DMF several times. The extract was evaporated under vacuum at 60°C and then isopropanol was added. The solid product so formed was collected by filtration, washed with isopropanol and dried. Yield 3.0 g (66%), yellow solid, m.p. >300°C. ^{1}H NMR spectrum (400 MHz, DMSO-d_6), δ, ppm (J, Hz): 5.50 (4H, s, NH_2), 6.69 (2H, d, J=8.4, 5-H), 7.38 (2H, d, J=8.6, 6-H), 7.58 (2H, d, J=1.6, 2-H). Found, m/z: 406.9491 $[M-2Na]^-$. $C_{12}H_{10}N_2Na_2O_6S_4$. Calculated, m/z: 406.9495.

2.2. Methods for analyzing chemical structures

For the analysis of bis(2-amino-5-*R*-phenyl)disulfides (APhDS), high-performance liquid chromatography with high-resolution mass spectrometric detection using electrospray ionization (HPLC-HRMS-ESI) combined with UV detection was employed. The setup consisted of an Agilent 1269 Infinity liquid chromatograph and an Agilent 6230 TOF LC/MS time-of-flight mass detector. Quantitative determination was performed using the internal standard method. ^{1}H NMR spectra were recorded on a Bruker AV600 (600.13 MHz) and Bruker DPX400 (400.1 MHz) spectrometers in DMSO-d_6 with TMS as the internal standard.

2.3. Electroless nickel bath

The main chemical composition of the bath and operating conditions are given in Table 3. Nickel hexahydrate chloride was used as the nickel source. Sodium hypophosphite was utilized as the reducing agent, also serving as the phosphorus source in the coating. Glyoxylic acid was employed as a complexing agent to control the release rate of free metal ions in the reduction reaction. Sodium acetate was used as a buffer. Organic disulfides (APhDS), listed in Table 2, were used as stabilizers to prevent bath decomposition. The concentration of organic compounds (ODS) ranged from $3.16\cdot10^{-7}$ to $1\cdot10^{-4}$ mol/L. The solution temperature for coating deposition was maintained at 80±1°C throughout the experiment using a water bath (LOIP LB-140). The bath pH was kept at 5.50 by adding sodium hydroxide (Ionmeter I-160MI). The deposition time for each sample was 30 minutes.

Table 3. Electroless nickel plating bath composition and operating conditions.

Composition and operating conditions	Values
$NiCl_2 \cdot 6H_2O$	20 g/L
NH_2CH_2COOH	15 g/L
$NaH_2PO_2 \cdot H_2O$	25 g/L
CH_3COONa	10 g/L
APhDS	3.16×10^{-7} to 1×10^{-4} mol/L
pH	5.5±0.1
Temperature	80±1°C
Deposition time	30 min

2.4. Measurement of deposition rate

Deposition experiments was performed on rectangular copper samples of grade M1 measuring 30 mm×25 mm×1 mm, that were used as a substrate. The copper samples were pre-treated as follows: degreasing in ethyl alcohol, rinsing in distilled water, etching, double rinsing in distilled water, and finally drying in air. Etching was performed twice for 2-3 seconds in a solution with the following composition: H_2SO_4:HNO_3:HCl/900:410:5 (g/L). The samples were weighed on analytical scales (A&D GR-300, Japan) with an accuracy of 0.0001 g and immediately coated with nickel.

An amount of 80.0 ml of the plating solution was added to the beaker immersed in a NESLAB GP-200 temperature regulated water bath.

The coating deposition was conducted in a heat-resistant 100 ml beaker immersed in a water bath.75 ml of the plating solution were added to the beaker. When the temperature reached the set value, the pre-treated copper foil substrate was immersed in the solution. Catalytic nickel plating was induced on the surface of copper by touching a steel rod, onto which a Ni–P deposit had been previously applied. The nickel plating solution was not stirred during the deposition process. After 30 minutes, the sample was removed, rinsed with distilled water, dried in air, and weighed on analytical scales.

The deposition rate of Ni–P coating (V, μm/h) was determined by the gravimetric method and calculated using the formula:

$$V = \frac{m_2 - m_1}{78.5 \cdot 10^{-3} \cdot S \cdot t},$$

where m_1 is the mass of the sample before deposition, g; m_2 is the mass of the sample after deposition, g; t is the nickel plating time, h; S is the surface area to be covered, dm^2; $78.5 \cdot 10^{-3}$ $g/(dm^2 \cdot h) = 1$ μm/h.

The experimental results presented in this study represent the average values of triple measurements.

2.5. Analysis of Ni–P coatings

The surface morphology of the obtained Ni–P coatings was investigated using a scanning electron microscope JSM-6510LV JEOL. The elemental composition of the nickel coatings was studied using X-ray microanalysis with an attachment to the electron microscope INCA Energy 250. X-ray structural analysis of Ni–P coatings was performed at room temperature using a DRON-4.07 diffractometer with CuKα radiation. The research was conducted at the Central Collective Use Center of Voronezh State University.

2.6. Bath stability test

Palladium salts are widely used to initiate the precipitation reaction in the volume of electrolytes [23–27]. This approach was used to determine the influence of the APhDS concentrations on bath stability. The tests were conducted at a temperature of 80±1°C. To 25 ml of the test solution, the catalyst in the form of a solution of $PdCl_2$ salt was added with continuous stirring. The amount of catalyst was adjusted so that the solution decomposition time was 15–20 seconds, after which the solution became opaque with a dark green color. In order to minimize solution dilution, the added volume of palladium salt did not exceed 300 μl. Solutions with different concentrations of $PdCl_2$ were used for this purpose: 0.25, 1.00, 4.00 and 8.00 g/l. Experiments were conducted at least three times to confirm the reproducibility of the results.

3. Results and Discussion

3.1. Deposition rate

The deposition rate of electroless Ni–P coatings was measured in the presence of organic additives APhDS (Table 2). The investigated concentration range was $3.16 \cdot 10^{-7}$ to $1 \cdot 10^{-4}$ mol/L. The effect of APhDS concentrations on the deposition rate of Ni–P coatings is presented in Table 4, indicating that nearly all additives up to a concentration of $1 \cdot 10^{-5}$ mol/L gradually increase the deposition rate. However, singling out one of them with the most accelerating action is difficult. Further increasing the concentration of the additive leads to a decrease in the rate, ultimately halting the process entirely at a concentration of $1 \cdot 10^{-4}$ mol/L.

The gradual increase in nickel deposition rate followed by a decrease is in line with previously observed results. Thus, research has shown that the addition of thiourea can lower the activation energy of the electroless nickel deposition reaction [28]. Radiochemical studies of thiourea during the electroless nickel process have indicated that the effect of thiourea on the nickel deposition rate is determined by two distinct mechanisms depending on the concentration of thiourea [29, 30]. Further discoveries have shown that thiourea derivatives increase the rate of electroless deposition by effective adsorption on the metal surface. Additionally, the nickel reduction by hypophosphite as a reducing agent is governed by a chemical mechanism.

Table 4. Influence of APhDS concentrations on the rate of Ni–P coatings.

	Deposition rate of Ni–P coating, μm/h						
Concentration of the additive, lg*C* (mol/L)	**0**	**–6.5**	**–6.0**	**–5.5**	**–5.0**	**–4.5**	**–4.0**
4a (R = H)		13.3	14.1	14.6	15.2	13.4	0
4b (R = CH_3O)		13.6	13.6	14.5	14.5	13.9	0
4c (R = Cl)		13.4	13.4	13.8	14.1	12.9	0
4d (R = F)	13.1	14.0	13.8	14.4	14.5	13.5	0
4e (R = COOH)		13.4	14.3	14.6	14.5	14.2	0
4f (R = CH_3)		14.2	14.3	14.4	14.5	14.0	0
4g (R = SO_3Na)		13.2	14.0	14.3	14.3	13.7	0

Other experimental results have shown that sulfur-containing organic compounds, including thiourea, mainly affect the anodic reaction, accelerating the entire deposition process. A hypothesis was formulated suggesting that these compounds boost hypophosphite adsorption, thereby accelerating the overall anodic reaction. The more electron-donating properties the compounds have, the higher their adsorption capacity and the stronger the blocking effect, which can stabilize the electrolyte [13, 14, 32]. Like thiourea, the –S–S– group can also contribute to the polarization of the P–H bond in hypophosphite ions, facilitated by the sulfur atom, which is the most polarizable atom with the lowest electronegativity. This facilitates electron transfer to nickel ions and accelerates the coating deposition rate. The polarizing ability of sulfur atoms in APhDS molecules may be influenced by the position of substituents in the benzene ring. Ortho-position of the amino group enhances electronic density on sulfur atoms, thereby strengthening the molecule's polarization properties. It was found that regardless of their nature, substituents in the 5^{th} position of APhDS do not influence the deposition rate of Ni–P coatings. This could be due to the fact that both electron-donating substituents (CH_3O–, CH_3–) and electron-accepting substituents (–SO_3Na, –COOH, –Cl, –F) in the meta-position relative to the sulfur atom insignificantly affect the electronic density on the key disulfide fragment sulfur atoms.

The authors [33] have proposed a mechanism by which thiourea accelerates and inhibits the deposition of electroless Ni–P coating. It is suggested that a similar acceleration mechanism could be possible for APhDS disulfides. Figure 3 shows a schematic diagram of the deposition of Ni–P coating with the addition of APhDS. Initially, the disulfide is reduced by hypophosphite to a reactive aminothiophenol, which is then oxidized to a free radical ([2-NH_2-5-*R*-C_6H_4S*]) through a charge transfer process. In the second stage, the free radical of aminothiophenol reacts with another free radical, thereby regenerating the original APhDS. This proposition is supported by research confirming that thiourea dimer acts as an electron transfer agent. For this, the authors [34] synthesized thiourea disulfide and used it in the

nickel deposition process. In all experiments, a similar increase in the deposition rate was observed as in the case of thiourea. Thus, the reaction process of accelerating deposition in the presence of APhDS can be represented by Equations (1) and (2).

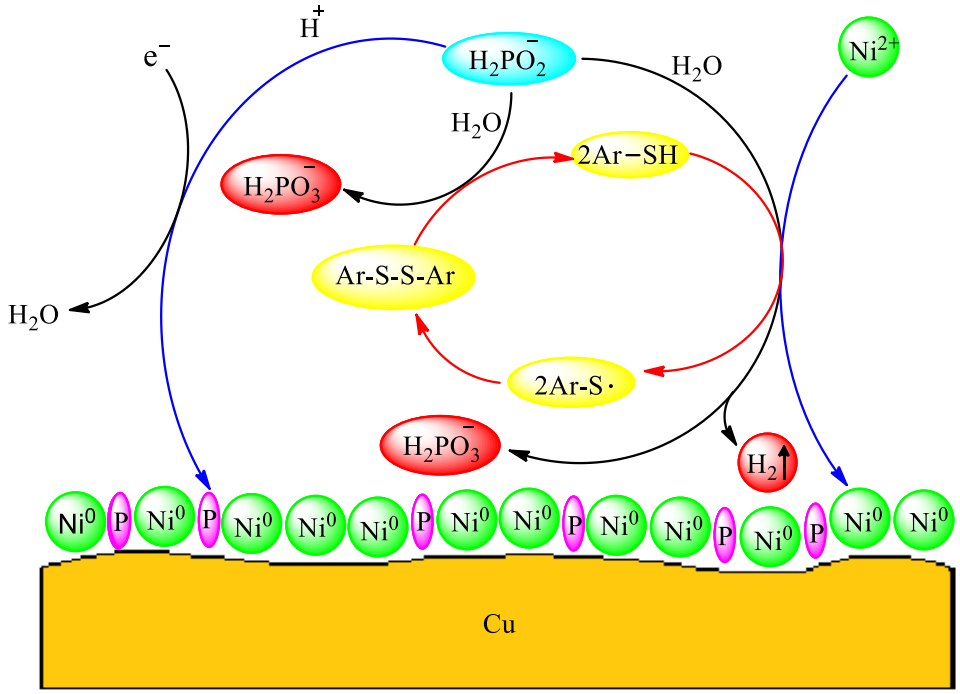

Figure 3. Deposition mechanism of electroless plating in the presence of APhDS.

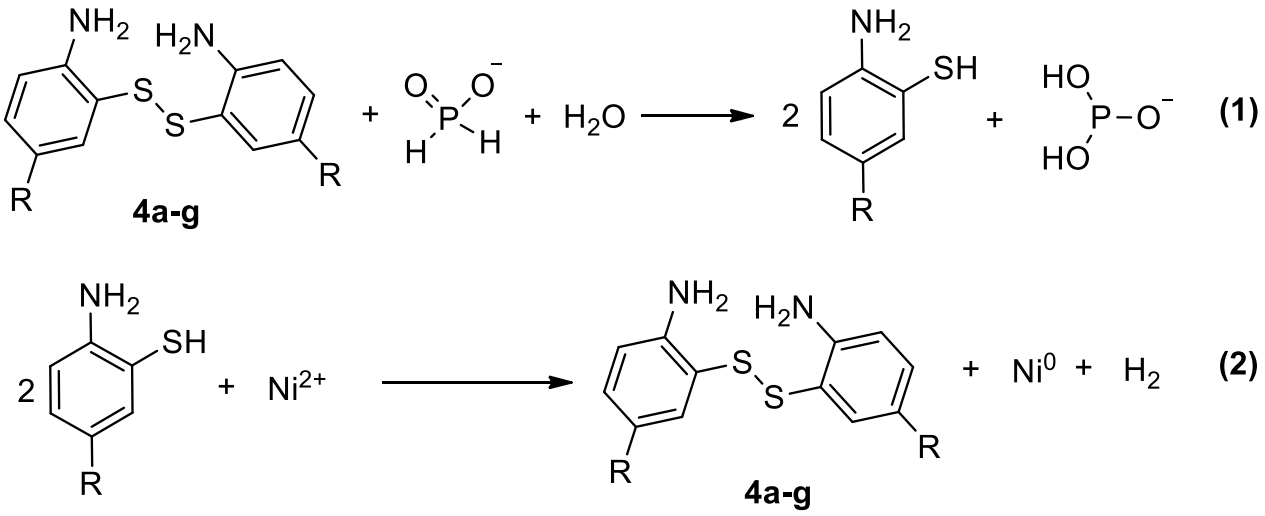

It is evident that the deposition of electroless Ni–P coatings in the presence of additives can also be influenced by other competing mechanisms. One of these mechanisms involves the adsorption of additives on the catalytic sites of the metal surface. In the initial phase, hypophosphite is adsorbed on these catalytic surfaces, leading to its subsequent reorientation and homolytic cleavage of the P–H bond [35]. With an increase in additive concentration, the number of catalytic centers decreases due to the formation of a thin film of additives on

the metal surface. This film impedes access, inhibits the oxidation of hypophosphite ions, and consequently hampers the deposition of Ni–P coating.

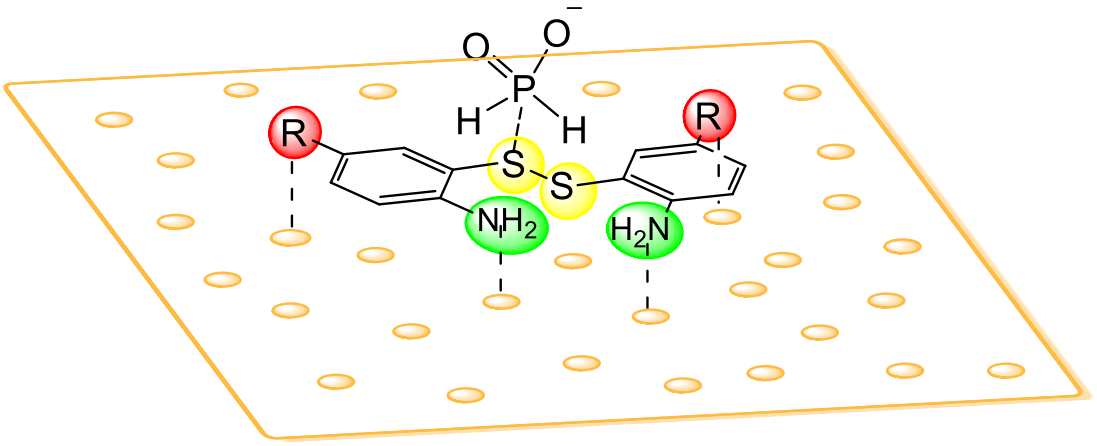

Figure 4. Adsorption of hypophosphite and APhDS on the catalytic surface.

As a result, it can be concluded that at low concentrations of the APhDS additive in the range of $3.16 \cdot 10^{-7} – 3.16 \cdot 10^{-5}$ mol/L, the rate of surface coating increases due to a catalysis process, which involves the formation of a reactive intermediate that facilitates the electron transfer to Ni^{2+} ions. Increasing the concentration of APhDS leads to a decrease in the catalytic activity of the surface due to a reduction in the number of active centers on the surface and the predominance of the inhibitory effect of additive surface adsorption on the deposition process. Additionally, functional substituents of the benzene ring may promote the formation of surface complexes, which can enhance the adsorption of APhDS on the metal surface (Figure 4).

3.2. Bath stability

Within the framework of this study, it was equally important to investigate the impact of APhDS additives on the volume reaction rate, *i.e.*, assess their stabilizing properties and determine the effective concentration for the specific chemical composition of the bath. The test results are presented in Table 5, indicating that the influence of APhDS on the bath stability initiates at a concentration of $1 \cdot 10^{-6}$ mol/L APhDS. As the stabilizer concentration increases to $3.16 \cdot 10^{-5}$ mol/L, the required $PdCl_2$ concentration escalates to 15–18 mg/L. At a stabilizer concentration of $1 \cdot 10^{-4}$ mol/L, bath stability increases significantly; however, this does not hold practical significance as, at this APhDS concentration under pH 5.5 and 80°C conditions, the precipitation of Ni–P does not occur. The most practically significant concentration range for enhancing bath stability lies between $1 \cdot 10^{-5}$ and $3.16 \cdot 10^{-5}$ mol/L of APhDS. Furthermore, the results indicate that there are minimal differences in stability among the additives, suggesting that substituents in the 5th position of APhDS do not influence the complexing properties with both Pd^{2+} ions and Ni metallic embryos.

Table 5. The minimum concentration of $PdCl_2$ at which spontaneous electrolyte decomposition initiates.

Concentration of the additive, lg*C* (mol/L)		**0**	**–6.0**	**–5.0**	**–4.5**	**–4.0**
The minimum concentration of $PlCl_2$ (in mg/L) required to initiate the spontaneous decomposition of the electrolyte:	**4a** (R = H)	1	2	7	17	50
	4b (R = CH_3O)		2	6	16	46
	4c (R = Cl)		3	7	17	24*
	4d (R = F)		2	6	15	46
	4e (R = COOH)		2	6	17	45
	4f (R = CH_3)		3	8	18	49
	4g (R = SO_3Na)		2	7	17	52

*(the additive partially precipitates)

3.3. Deposit morphology

The surface morphology of electroless nickel deposition is significantly influenced by the characteristics of the plating solution [26]. Without APhDS, the Ni–P coating exhibits a distinctive spherical nodular structure, as shown in Figure 4.

The formation of nodules is a prominent trait of electroless Ni–P coatings. The rapid nucleation, Ni_3P phase precipitation in the absence of stabilizers, and subsequent Ni–P growth all contribute to nodule formation on the coatings. Potential impacts on the surface morphology of Ni–P electroless coatings may arise from the adsorption of additives on the surface and facets of growing crystals. Authors [36] suggest that hydrogenolysis of C–S and S=O bonds and the adsorption of resulting sulfur anions impede crystal growth in specific directions. Thus, the predominance of the (100) texture in the nickel deposit obtained by galvanic method is explained by the specific adsorption of sulfur anions on the crystallographic direction (110), thereby hindering growth in that plane. It has also been observed that the use of thio-derived stabilizers like mercaptobenzothiazole [37] or thiourea [38] at concentrations exceeding 2 ppm can promote the development of columnar cauliflower morphology.

Therefore, the use of APhDS as stabilizers in the electroless nickel plating bath can affect the growth of crystals in a specific orientation. A comparative analysis of the influence of APhDS additives at different concentrations on the morphology of coatings is shown in Figure 6. Microphotographs of the surface of the electroless Ni–P deposit sample obtained without APhDS are shown in Figure 5.

Figure 6 shows that at a concentration of $1 \cdot 10^{-6}$ mol/L of APhDS with H– and CH_3– substituents, the surface exhibits a more pronounced nodular structure, with grain boundaries being sufficiently blurred, resembling an “orange peel” texture. When the concentration of these additives is increased to 10^{-5} mol/L, the nodular structure transitions into a granular structure, with an average grain size of 1.5–2.0 μm and the inclusion of large grains up to

3 μm in size. Further increasing the additive concentration to $3.16 \cdot 10^{-5}$ mol/L leads to the merging of small grains into larger ones up to 2–3 μm in size. APhDS with –F and –Cl substituents at a concentration of 10^{-6} mol/L results in the surface exhibiting a continuous granular structure, with an average grain size of 1.5–1.7 μm. With an increase in the concentration of halogen derivatives of APhDS, large crystals of 4–5 μm with inclusions of smaller grains measuring 0.7–1.2 μm are formed, which completely disappear at a concentration of $3.16 \cdot 10^{-5}$ mol/L. When using APhDS with substituents –COOH and $-SO_3Na$ at a concentration of $1 \cdot 10^{-6}$ and $1 \cdot 10^{-5}$ mol/L, the surface becomes very smooth. Further increasing the concentration of these additives to $3.16 \cdot 10^{-5}$ mol/L results in the formation of rare cluster-like particles measuring 2.0–3.5 μm.

Although in the presence of low concentrations of APhDS ($1 \cdot 10^{-6}$ mol/L) with different substituents, the rate of coating application is almost identical to the deposition rate without additives, we have observed their influence on surface morphology. When using them, the surface is smoothened, especially noticeable with oxygen-containing substituents like CH_3O–, –COOH, and $-SO_3Na$. This effect is likely due to the orientation-specific adsorption of these additives on the active crystal centers in conditions of limited quantity in the electrolyte, facilitated by oxygen atoms. This leads to the inhibition of columnar crystal growth, causing lateral growth to predominate. Conversely, halogen substituents contribute to inhibiting lateral growth. The morphology obtained with CH_3– substituent is particularly similar to the unsubstituted APhDS, explaining the minimal influence of the methyl group on the molecule's adsorption capacity. With an increase in APhDS concentration in the electrolyte, the number of adsorbed molecules on the surface increases. The enhanced rate of Ni–P coating application in the presence of $1 \cdot 10^{-5}$ mol/L APhDS further supports this observation. The increased presence of the stabilizer on the surface restricts lateral growth of the Ni–P layer, predominantly leading to the formation of columnar deposits. At an additive concentration of $3.16 \cdot 10^{-5}$ mol/L, the coating rate starts to decrease, indicating a higher quantity of adsorbed APhDS molecules on the active centers of the deposited surface. The amplified inhibition of both lateral and columnar particle growth results in the appearance of larger crystals on the surface. This correlation is observed for all investigated substituents.

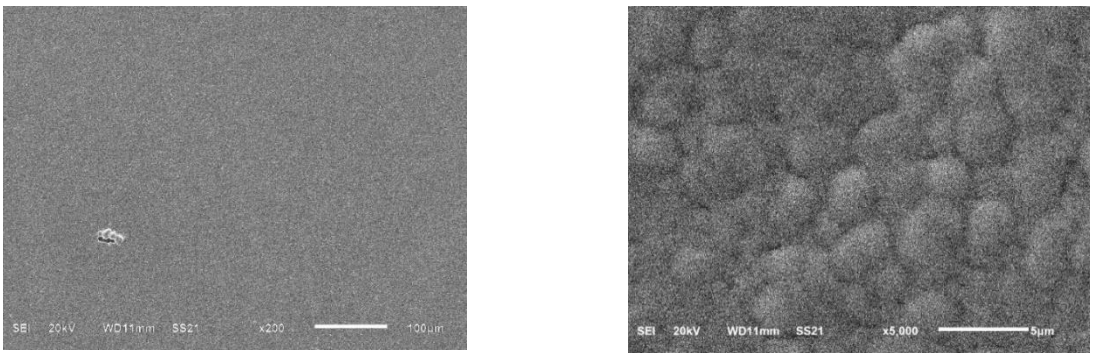

a b

Figure 5. SEM micrographs of the electroless Ni–P deposits obtained without APhDS at magnification: a – ×200, b – ×5000.

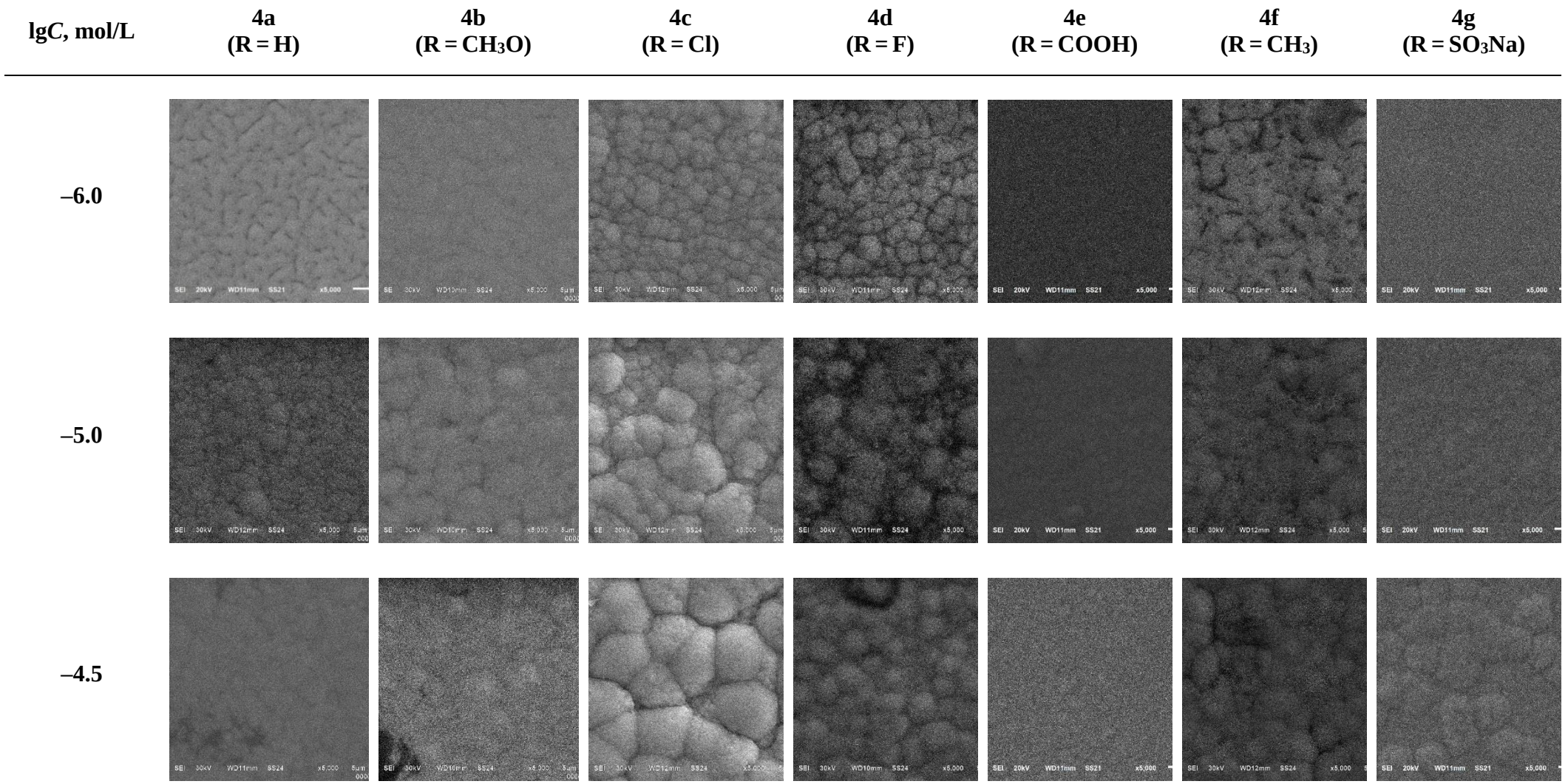

Figure 6. Comparative analysis of SEM microphotographs of Ni–P coating surfaces deposited using APhDS additives at 5000x magnification.

3.4. Elemental composition of the deposit

It is known that in the process of electroless nickel plating, phosphorus is deposited along with nickel [39–40]. The influence of stabilizers on the phosphorus content in the coating was studied using X-ray diffraction. Figure 7 shows the characteristic results of the elemental analysis of the investigated Ni, P-coatings electroless deposited using APhDS additives. The relative concentrations of Ni and P in the obtained samples are given in Table 6. The coating deposited without the use of organic additives contains 13.34 at.% phosphorus, classifying it as a coating with an average phosphorus content [41]. With an APhDS concentration of $1 \cdot 10^{-6}$ mol/L, the phosphorus content (~12–13 at.%) remains almost unchanged compared to the coating obtained without the additive (13.34 at.%). As the APhDS concentration increases to $1 \cdot 10^{-5}$ mol/L, the effect of the additive on the phosphorus content in the coatings becomes apparent. Under these conditions, there is a redistribution of the Ni and P concentration towards reducing the phosphorus content to 9.41–10.52 at.%, except for the coating obtained with the untreated APhDS 4a, which shows a higher P content (12.12 at.%).

The reduction reactions of Ni and P compete with each other, as they require either electrons or adsorbed hydrogen atoms [39, 40]. Therefore, as the nickel deposition rate increases in the presence of an accelerator, the phosphorus content in the coatings decreases. As the concentration of APhDS additives is further increased to $3.16 \cdot 10^{-5}$ mol/L, despite the reduction in nickel deposition rate (Table 4), the coatings exhibit even lower phosphorus content (5.62–7.41 at.%). This is likely due to the adsorption of APhDS molecules partially blocking the access of hypophosphite molecules to adsorbed hydrogen atoms on the coating, leading to a reduction in phosphorus content according to the atomic hydrogen mechanism. APhDS with CH_3 and $-SO_3Na$ substituents, on the contrary, contribute to a slight increase in the phosphorus content, indicating specific adsorption behavior of these additives.

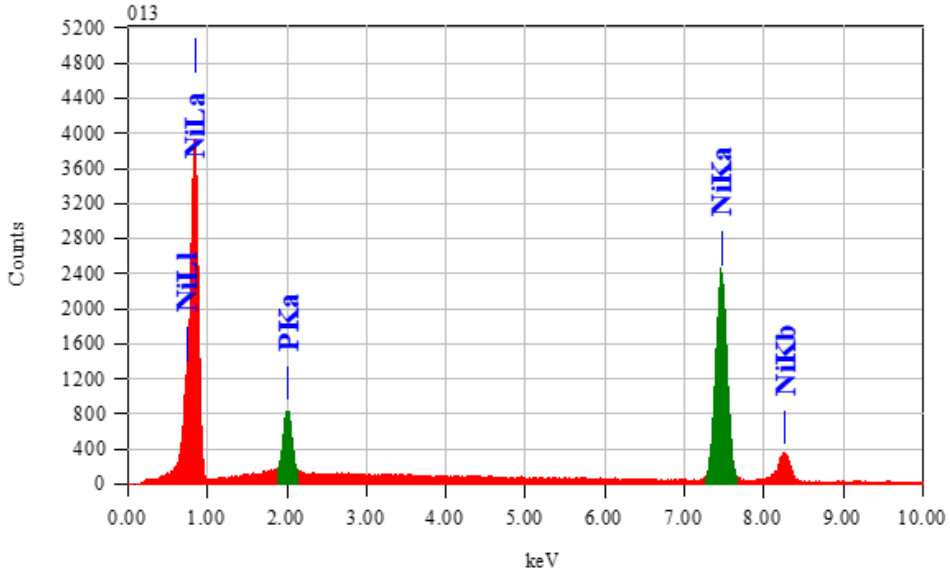

Figure 7. Typical results of elemental analysis of Ni–P coatings deposited on copper foil using APhDS additives.

Table 6. Composition of Ni–P coatings deposited using APhDS additives varies depending on their concentration.

Concentration of the additive, lg*C* (mol/L)	**0**		**–6.0**		**–5.0**		**–4.5**	
Elemental composition, at.%	**P**	**Ni**	**P**	**Ni**	**P**	**Ni**	**P**	**Ni**
4a (R = H)			12.75	87.25	12.12	87.88	7.41	92.59
4b (R = CH_3O)			11.96	88.04	10.50	89.50	5.97	94.03
4c (R = Cl)			13.55	86.45	10.52	89.48	7.34	92.66
4d (R = F)	13.34	86.66	13.02	86.98	10.45	86.45	6.63	93.37
4e (R = COOH)			11.38	88.62	9.99	90.01	5.60	94.40
4f (R = CH_3)			12.53	87.47	10.15	89.85	10.92	89.08
4g (R = SO_3Na)			11.85	88.15	9.41	90.59	9.68	90.32

3.5 X-ray diffraction analysis of the electroless Ni–P layers

It is known that an increase in phosphorus content in Ni–P coatings is accompanied by the amorphization of their structure [42], suggesting that the electroless Ni–P deposits can be either polycrystalline or amorphous. Thus, the phosphorus content is one of the crucial factors determining the structure of the coatings.

The diffraction patterns of the Ni–P deposits obtained using APhDS additives with different contents are presented in Figure 7. The reflexes observed at angles of 2Θ=43.36, 50.48, 74.19, 89.98 correspond to reflections from the planes of the Cu substrate (111), (200), (220), (311) respectively [ICDD 00-004-0836]. The broad peaks in the angular range of 2Θ=44.66, 51.83 belong to the investigated nickel coating, corresponding to reflections from the (111) and (200) Ni planes with a face-centered cubic (FCC) lattice [ICDD 00-004-0850].

In the X-ray diffraction pattern of the Ni–P coating obtained in the absence of additives, a single broad peak centered at 44.5° 2Θ is observed, indicating the amorphous nature of the coating. According to the X-ray diffraction data, the addition of AFDS to the electrolyte does not significantly affect the crystalline structure of the deposited coatings. With an increase in the additive concentration, there is a slight increase in the crystallinity of the coatings, manifested by a slight narrowing of the reflection line from the Ni (111) planes and an increase in the intensity of the reflection line from the Ni (200) planes. The decrease in phosphorus content in the coatings also supports this observation. These findings are consistent with studies on thiourea. The authors [43] noted that an increase in thiourea concentration enhances the crystallization of the Ni–P chemical coating. Reflection lines from the Ni (111) planes are observed at 0.25 ppm of thiourea, while reflections from the Ni (200) planes become noticeable with an increase in thiourea concentration up to 3 ppm.

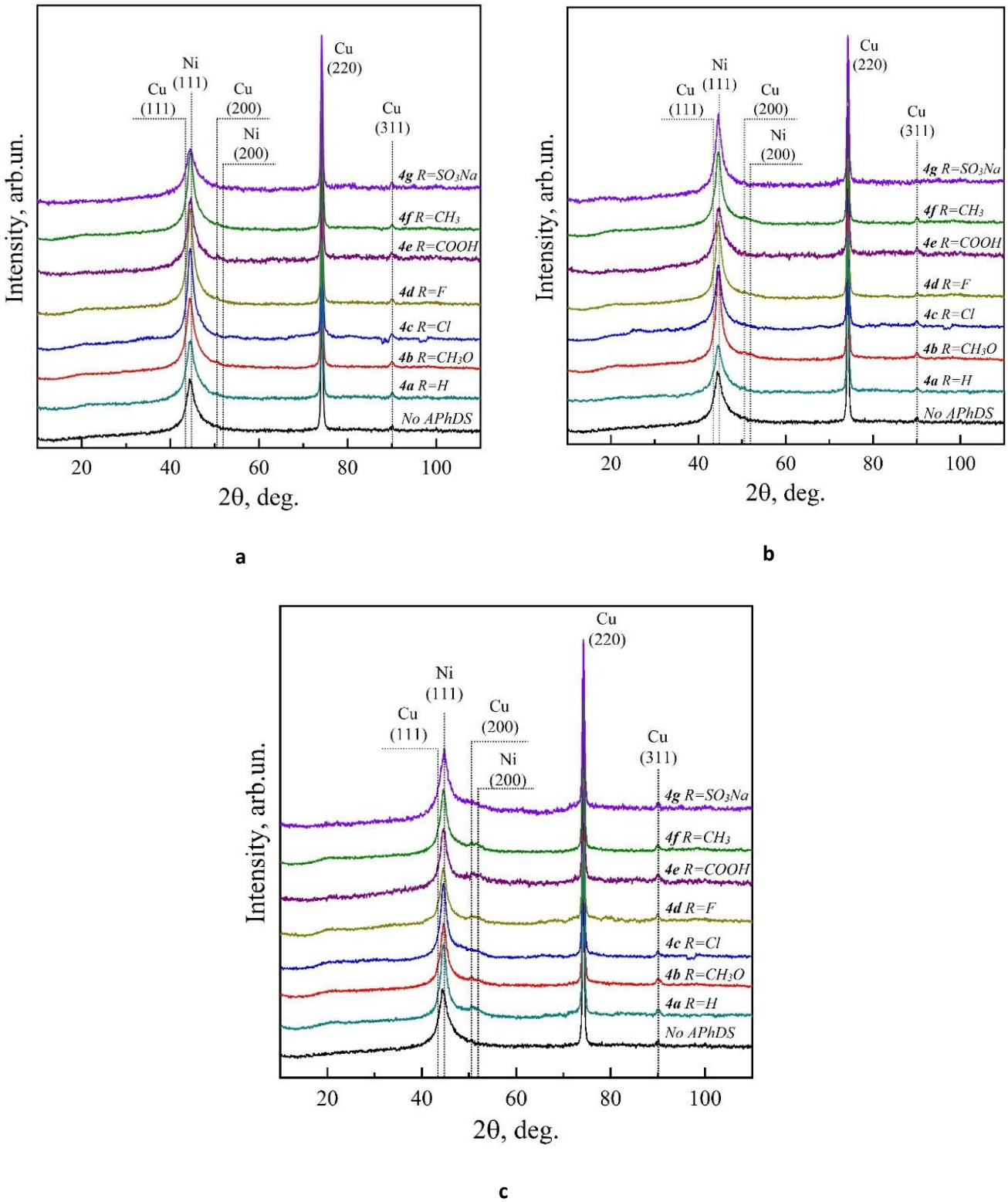

Figure 8. X-ray diffraction patterns of coatings deposited without the use of organic additives and using APhDS at a concentration: a) $1 \cdot 10^{-6}$ mol/L, b) $1 \cdot 10^{-5}$ mol/L, c) $3.16 \cdot 10^{-5}$ mol/L within the angular range of 10–110 degrees 2Θ.

Acknowledgments

The study received financial support from the Ministry of Science and Higher Education of the Russian Federation within the framework of State Contract with universities regarding scientific research in 2022–2024, project No. FZGU-2022-0003.

Conclusion

The effect of substituents in APhDS on the deposition processes and properties of Ni–P coatings studied in this paper. It has been found that all additives in the concentration range of about $3.16 \cdot 10^{-6}$ to $3.16 \cdot 10^{-4}$ mol/L exhibit catalytic activity and contribute to an increase in the deposition rate of coatings. Notably, the disulfide group emerges as a key driver of this acceleration, while the influence of other substituents remains relatively minor. At higher concentrations, inhibiting the process is observed, leading to its complete cessation. Functional substituents of the benzene ring can promote the formation of surface complexes, which may enhance APhDS adsorption on the metal surface and increase the stability of the nickel plating solution with the growth of additive concentration.

The influence of additives on the composition of coatings has been established: with increasing additive concentration, a decrease in phosphorus content in the coating is observed, and crystallinity increases compared to the solution without additives. The greatest impact of additives lies in the change of deposit morphology. At an additive concentration of $1 \cdot 10^{-6}$ mol/L, all coatings exhibit a smoother structure than in their absence. However, further increasing the additive concentration leads to surface development.

The obtained data on deposition rates and electrolyte stability indicates the potential use of APhDS additives in electroless nickel-plating solutions. Details on coating structure, morphology, and composition could be leveraged to create coatings with specific functional properties, such as corrosion resistance, by selecting additives with different substituents.

References

1. A. Brenner and G.E. Riddell, Nickel plating on steel by chemical reduction, *J. Res. Natl. Bur. Stand.*, 1946, **37**, no. 1, 31.
2. T.C. Wei, T.C. Pan, C.M. Chen, K.C. Lai and C.H. Wu, Annealing-free adhesive electroless deposition of a nickel/phosphorous layer on a silane-compound-modified Si wafer, *Electrochem. Commun.*, 2015, **54**, 6–9. doi: 10.1016/j.elecom.2015.02.009
3. M. Momenzadeh and S.Sanjabi, The effect of TiO_2 nanoparticle codeposition on microstructure and corrosion resistance of electroless Ni–P coating, *Mater. Corros.*, 2012, **63**, no. 7, 614–619. doi: 10.1002/maco.201005985
4. Q. Qi, Y. Wang, X. Ding, W. Wang, R. Xu and D. Yu, High-electromagnetic-shielding cotton fabric prepared using multiwall carbon nanotubes/nickel–phosphorus electroless plating, *Appl. Organomet. Chem.*, 2020, **34**, no. 3, 5434–5445. doi: 10.1002/aoc.5434

5. F.B. Mainier, M.P.C. Fonseca, S.S. Tavares and J.M. Pardal, Quality of electroless Ni–P (nickel–phosphorus) coatings applied in oil production equipment with salinity, *J. Mater. Sci. Chem. Eng*., 2013, **1**. no. 6, 1–8. doi: 10.4236/msce.2013.16001
6. N. Feldstein and P.R. Amodio, Anionic inhibition in electroless plating, *J. Electrochem. Soc*., 1970, **117**, no. 9, 1110. doi: 10.1016/j.matchemphys.2005.10.001
7. H.P. Liu, N. Li, S.F. Bi, D.Y. Li and Z.L. Zou, Effect of organic additives on the corrosion resistance properties of electroless nickel deposits, *Thin solid films*, 2008, **516**, no. 8, 1883–1889. doi: 10.1016/j.tsf.2007.10.008
8. A.R. Rahimi, H. Modarres and M. Abdouss, Study on morphology and corrosion resistance of electroless Ni–P coatings, *Surf. Eng*., 2009, **25**, no. 5, 367–371. doi: 10.1179/174329409X37927
9. K. Wang, L. Hong and Z.L. Liu, Investigation into the roles of sulfur-containing amino acids in electroless nickel plating bath, *Ind. Eng. Chem. Res*., 2008, **47**, no. 17, 6517–6524. doi: 10.1021/ie800456b
10. A.O. Gezerman and B.D. Çorbacıoğlu, 2-mercaptobenzimidazole, 2-mercaptobenzothiazole, and thioglycolic acid in an electroless nickel-plating bath, *J. Chem*., 2015, **2015**. doi: 10.1155/2015/872516
11. P. Balaramesh, S. Jayalakshmi, S.A. Fdo, V. Anitha and P. Venkatesh, Influence of organosulphur additives on autocatalytic copper thin film deposition, *Mater. Today: Proc*., 2021, **47**, 2020–2024. doi: 10.1016/j.matpr.2021.04.212
12. N.V. Sotskaya, O.V. Dolgikh and E.I. Ryabinina, Catalytic activity of nickel alloys in anodic oxidation of the hypophosphite ion as a function of their composition, *Russ. J. Electrochem*., 2005, **41**, 866–873. doi: 10.1007/s11175-005-0146-4
13. N.V. Sotskaya, T.A. Kravchenko, E.I. Ryabinina and O.V. Bocharova, Anodic Oxidation of Hypophosphite on a Nickel–Phosphorus Electrode in the Presence of Some Organic Compounds, *Russ. J. Electrochem*., 2003, **39**, 960–966. doi: 10.1023/A:1025776005148
14. N.V. Sotskaya, E.I. Ryabinina, T.A. Kravchenko and K.S. Shikhaliev, Kinetics of electroless plating of Ni–P alloys with organic additives containing –S–S– fragments, *Prot. Met*., 2003, 39, 250–254. doi: 10.1023/A:1023967120687
15. A.L. Mnjoyan, Syntheses of heterocyclic compounds: vol. 6, Yerevan, Publishing House of the Academy of Sciences of the Armenian SSR, 1964, p. 90.
16. A. Furlan, F. Colombo, A. Kover, N. Issaly, C. Tintori, L. Angeli, V. Leroux, S. Letard, M. Amat, Y. Asses, B. Maigret, P. Dubreuil, M. Botta, R. Dono, J. Bosch, O. Piccolo, D. Passarella and F. Maina, Identification of new aminoacid amides containing the imidazo[2,1-*b*]benzothiazol-2-ylphenyl moiety as inhibitors of tumorigenesis by oncogenic Met signaling, *Eur. J. Med. Chem*., 2012, **47**, 239–254. doi: 10.1016/j.ejmech.2011.10.051
17. R.V. Patel, P. Kumari, D.P. Rajani and K.H. Chikhalia, Synthesis of coumarin-based 1,3,4-oxadiazol-2ylthio-*N*-phenyl/benzothiazolyl acetamides as antimicrobial and

antituberculosis agents, *Med. Chem. Res*., 2013, **22**, 195–210. doi: 10.1007/s00044-012-0026-x
18. W. Hirose, K. Sato and A. Matsuda, Fluorescence Properties of 5-(5,6-Dimethoxybenzothiazol-2-yl)-2′-deoxyuridine (dbtU) and Oligodeoxyribonucleotides Containing dbtU, *Eur. J. Org. Chem*., 2011, 6206–6217. doi: 10.1002/ejoc.201100818
19. S.K. Abbas, H.D. Hanoon, Z.F. Abbas, K.A. Hussein and S.M. Radhi, Synthesis, spectral characteristics, and biological activity of 1,3-oxazepines and 1,3-oxazepanes derived from 6-nitrobenzothiazol-2-amine, *Russ. J. Org. Chem*., 2020, **56**, 327–331. doi: 10.1134/S1070428020020244
20. R. Kruszynski and A. Trzesowska-Kruszynska, 2,3-Dihydro-1,3-benzothiazol-2-iminium monohydrogen sulfate and 2-iminio-2,3-dihydro-1,3-benzothiazole-6-sulfonate: a combined structural and theoretical study, *Acta Crystallogr*., *Sect. C: Cryst. Struct. Commun*., 2009, **65**, no. 12, o624–o629. doi: 10.1107/S0108270109045673
21. H.U. Blank, T. Pfister and R. Putter, *US Patent*, *4375562, C07C*, 1983.
22. A. Shokrollahi, A. Abbaspour, M. Ghaedi, A.N. Haghighi, A.H. Kianfar and M. Ranjbar, Construction of a new Cu^{2+} coated wire ion selective electrode based on 2-((2-(2-(2-(2-hydroxy-5-methoxybenzylideneamino)phenyl)disufanyl)phenylimino)methyl)-4-methoxyphenol Schiff base, *Talanta*, 2011, **84**, no. 1, 34–41. doi: 10.1016/j.talanta.2010.12.002
23. M. Gulla and C. Savas, *US Patent, 4189324, C23C*, 1980.
24. E.R. Ramirez, *US Patent, 2884344, C23C*, 1959.
25. S.S. Abd El-Rehim, M. Shaffei, N. El-Ibiari and S.A. Halem, Effect of additives on plating rate and bath stability of electroless deposition of nickel-phosphorus-boron on aluminum, *J. Met. Finish*., 1996, **94**, no. 12, 29–33. doi: 10.1016/S0026-0576(96)80087-0
26. M.R. Gad and A. El-Magd, Additives for electroless nickel alloy coating processes, *J. Met. Finish*., 2001, **99**, no. 2, 77–83. doi: 10.1016/S0026-0576(01)81008-4
27. W.J. Cheong, B.L. Luan and D.W. Shoesmith, The effects of stabilizers on the bath stability of electroless Ni deposition and the deposit, *Appl. Surf. Sci*., 2004, **229**, no. 1–4, 282–300. doi: 10.1016/j.apsusc.2004.02.003
28. H. Ke-Ping and F. Jing-Li, Acceleration effect of electroless nickel deposition by thiourea, *Int. J. Chem. Kinet*., 1996, **28**. no. 4, 259–264. doi: 10.1002/(SICI)1097-4601(1996)28:4<259::AID-KIN3>3.0.CO;2-U
29. J.S. Sallo, J. Kivel and F.C. Albers, Radiochemical studies of thiourea in the electroless deposition process, *J. Electrochem. Soc*., 1963, **110**, no. 8, 890. doi: 10.1149/1.2425895
30. J. Kivel and J.S. Sallo, The effect of thiourea on alkaline electroless deposition, *J. Electrochem. Soc*., 1965, **112**, no. 12, 1201. doi: 10.1149/1.2423399
31. S. Karthikeyan, P.A. Jeeva, S. Narayanan, K.N. Srinivasan and X. Hu, Quantum mechanical approach for electroless plating process, *Surf. Eng*., 2012, **28**, no. 10, 743–746. doi: 10.1179/1743294412Y.0000000053

32. M. Kunimoto, K. Endo, H. Nakai and T. Homma, Acceleration effect of thiourea on the oxidation reaction of hypophosphite ion on Ni surface, *Electrochim. Acta*, 2013, **100**, 311–316. doi: 10.1016/j.electacta.2012.09.070
33. H. Xu, J. Brito and O.A. Sadik, Mechanism of stabilizer acceleration in electroless nickel at wirebond substrates, *J. Electrochem. Soc*., 2003, **150**, no. 11, C816. doi: 10.1149/1.1617307
34. J. Kivel and J.S. Sallo, The effect of thiourea on alkaline electroless deposition, *J. Electrochem. Soc*., 1965, **112**, no. 12, 1201. doi: 10.1149/1.2423399
35. M.E. Touhami, E. Chassaing and M. Cherkaoui, Modelisation of Ni–P electroless deposition in ammoniacal solutions, *Electrochim. acta*, 2003, **48**, no. 24, 3651–3658. doi: 10.1016/S0013-4686(03)00486-9
36. J. Macheras, D. Vouros, C. Kollia and N. Spyrellis, Nickel electro-crystallization: Influence of unsaturated organic additives on the mechanism of oriented crystal growth, *Trans. IMF*, 1996, **74**, no. 2, 55–58. doi: 10.1080/00202967.1996.11871093
37. G. Salvago and G. Fumagalli, Considerations on the corrosion resistance of metallic materials coated with electroless nickel, *Key Eng. Mater*., 1988, **20**, 1027–1034. doi: 10.4028/www.scientific.net/KEM.20-28.1027
38. W. Wu, J. Liu, N. Miao, J. Jiang, Y. Zhang, L. Zhang, N. Yuan, Q. Wang and L. Tang, Influence of thiourea on electroless Ni–P films deposited on silicon substrates, *J. Mater. Sci.: Mater. Electron*., 2019, **30**, 7717–7724. doi: 10.1007/s10854-019-01088-4
39. G.O. Mallory and J.B. HaJdu, *Electroless plating: fundamentals and applications*, William Andrew, New York, USA, 1990, p. 539.
40. R.C. Agarwala and V. Agarwala, Electroless alloy/composite coatings: A review, *Sadhana*, 2003, **28**, 475–493. doi: 10.1007/BF02706445
41. A. Salicio-Paz, I. Ugarte, J. Sort, E. Pellicer and E. García-Lecina, Full Optimization of an Electroless Nickel Solution: Boosting the Performance of Low-Phosphorous Coatings, *Materials*, 2021, **14**, no. 6, 1501. doi: 10.3390/ma14061501
42. I.V. Petukhov, M.G. Shcherban', N.E. Skryabina and L.N. Malinina, Corrosion and electrochemical behavior of Ni–P coatings in 0.5 M H_2SO_4, *Prot. Met*., 2002, **38**, 370–376. doi: 10.1023/A:1019669503487
43. K.L. Lin and J.W. Hwang, Effect of thiourea and lead acetate on the deposition of electroless nickel, *Mater. Chem. Phys*., 2002, **76**, no. 2, 204–211. doi: 10.1016/S0254-0584(01)00516-8

♦ ♦ ♦